Biosensors and Bioelectronics 126 (2019) 129–135

Contents lists available at ScienceDirect

Biosensors and Bioelectronics

journal homepage: www.elsevier.com/locate/bios

Two-photon semiconducting polymer nanoparticles as a new platform for imaging of intracellular pH variation

Biqing Bao, Zhenyuan Yang, Yunfei Liu, Yu Xu, Bingbing Gu, Jia Chen, Peng Su, Li Tong, Lianhui Wang*

Key Laboratory for Organic Electronics and Information Displays (KLOEID) & Jiangsu Key Laboratory for Biosensors, Institute of Advanced Materials (IAM), Jiangsu National Synergistic Innovation Center for Advanced Materials (SICAM), Nanjing University of Posts and Telecommunications, Nanjing 210023, Jiangsu, China

ARTICLE INFO

Keywords:
Semiconducting polymer nanoparticles
pH
Polydopamine
Probe

ABSTRACT

Intracellular pH (pHi) plays a crucial role in cell physiological and pathological processes. We herein report an efficient pH-sensitive sensor based on two-photon excitable semiconducting polymer nanoparticles (PFV/PSMA-DA NPs) for pHi sensing. PFV/PSMA NPs were functionalized with redox-active dopamine (DA) and the obtained PFV/PSMA-DA NPs showed sensitive and reversible pH response over the pH range of 5.0–9.0. Owning to the high biocompatibility and pH-responsive DA, PFV/PSMA-DA NPs show low cytotoxicity and the quantification and imaging of intracellular pH changes of HeLa cells were successfully realized. Moreover, the detection of intracellular pH fluctuation induced by redox species such as NAC (N-acetylcysteine) and H_2O_2 was also achieved by both one- and two-photon excitation of the PFV/PSMA-DA NPs probe. This work clearly shows that nanoprobe based on two-photon PFV/PSMA-DA NPs could serve as a promising platform for quantitatively monitoring the intracellular pH fluctuations.

1. Introduction

In recent years, intracellular pH (pHi) have become significantly important in many areas such as analytical chemistry, cellular biology and biomedicine (Hou et al., 2017; Wen et al., 2013). Among traditional techniques for pHi measurement, fluorescence technology have attracted considerable attention due to the advantages of high sensitivity, non-invasiveness and excellent spatiotemporal resolution (Thomas, 2015; Yin et al., 2015). Although several pH fluorescence sensors including quantum dots (QDs) (Bruni et al., 2017; Jung and Chen, 2018; D. Li et al., 2017; Nareoja et al., 2017), small organic dyes (W. Sun et al., 2016; Xu et al., 2016), and fluorescent proteins (Dennis et al., 2012; Miesenbock et al., 1998; Tantama et al., 2011) have been developed, there still exist a number of challenges that could greatly impede their practical biological applications. For example, conventional organic dyes are usually suffered from their poor water solubility and susceptibility to photobleaching (Ke et al., 2017). The long-term toxicity of quantum dots and up conversion nanoparticles may cause serious damage to living biosubstrates and impede their biological use and clinical implementation (Derfus et al., 2004).

In addition, most of the developed fluorescent probes for pHi sensing are one-photon excitation (usually in the UV region), which compromises their biomedical applications due to the strong tissue autofluorescence, large photodamage, and limited penetration depth owing to big self-absorption and scattering (J. Sun et al., 2016; Wang et al., 2017). Two-photon (TP) bioimaging with near-infrared wavelength excitation has been shown to offer numerous advantages over the general one-photon excitation due to their excellent properties such as higher spatial resolution, reduced photodamage and photobleaching, and deeper penetration depth (Kim and Cho, 2015; J. Li et al., 2017; Qian et al., 2016). To date, most previously report TP fluorescent probes are based on small organic two-photon absorption molecules and show poor cell permeability (Jiang et al., 2017). Therefore, it is highly desirable to develop two-photon-excited organic nanoparticle probes with excellent biocompatibility and stability for pHi sensing and imaging.

As organic macromolecules, semiconducting polymer nanoparticles (SPNs) have recently attracted great interest due to their signal amplification ability, high brightness under one- or two-photon excitation, excellent photostability, and low toxicity, which have demonstrated their usefulness in biosensing (Bao et al., 2015; Sun et al., 2017a), biological imaging (Chen et al., 2017; Sun et al., 2017b) and phototherapy (Peng and Chiu, 2015; Wu and Chiu, 2013; Yu et al., 2017). In this study, semiconducting polymer nanoparticles with one-, two-

* Corresponding author.
E-mail address: iamlhwang@njupt.edu.cn (L. Wang).

https://doi.org/10.1016/j.bios.2018.10.027
Received 3 September 2018; Received in revised form 30 September 2018; Accepted 13 October 2018
Available online 18 October 2018
0956-5663/

photon excitation properties have been prepared by reprecipitation of poly(9,9′-dioctylfluorene-2,7-ylene-vinylene-*co*-*alt*-1,4-phenylene) (PFV) and amphiphilic polymer poly(styrene-*co*-maleic anhydride) (PSMA). Biocompatible and pH-responsive molecule dopamine (DA) were conjugated to the surface of the PFV/PSMA NPs for pHi sensing and bioimaging. Quantitative determinations of intracellular pH changes of untreated HeLa cells and the pH fluctuations under different stimulus have been successfully realized both by one- and two-photon fluorescence microscopy.

2. Experimental section

2.1. Chemicals and reagents

Poly(styrene-*co*-maleic anhydride) (PSMA), Dopamine-hydrochloride(DA), N-(3-dimethylaminopropyl)-N-ethylcarbodiimide hydrochloride (EDC), tetrahydrofuran were purchased from Sigma Aldrich. DMEM, fetal bovine serum, penicillin-streptomycin solution, trypsin-EDTA solution, and 3-(4,5-dimethylthiazol-2-yl)-2,5-diphenyl tetrazolium bromide (MTT) were purchased from KeyGen Biotech. Co. Ltd. All water used to prepare buffer solution was obtained from a Milli-Q water system.

2.2. Characterization

Dynamic light scattering (DLS) data were collected by a Brookhaven ZetaPALS instrument. Transmission electron microscopy (TEM) images were obtained with a Hitachi HT7700 transmission electron microscope operating at 100 kV accelerating voltage. A Hitachi S-4800 scanning electron microscopy (SEM) was utilized to record SEM images. The atomic force microscopy (AFM) images were conducted on a Bruker Dimension Icon atomic force microscope with tapping mode. UV–visible absorption spectra were recorded using Shimadzu UV–vis 3600 spectrophotometer. Fluorescence spectra were collected on the RF-5301PC fluorescence Spectrophotometer. Confocal fluorescence imaging were performed on an Olympus Fluo-view 1000 instrument.

2.3. Preparation of PFV/PSMA-DA NPs

The semiconducting polymer nanoparticles were prepared using the reprecipitation method. In general, semiconducting polymer PFV were dissolved in tetrahydrofuran (THF) and mixed with a diluted THF solution of PSMA to produce a solution mixture with a PFV concentration of 16 μg/mL and a PSMA concentration of 3 μg/mL. Then a 2 mL quantity of the mixture was quickly added to 10 mL of Milli-Q water in a bath sonicator. After THF was removed by vacuum evaporation, the obtained solution was concentrated and filtered through a 0.22 μm filter. Bioconjugation between PFV/PSMA NPs and dopamine was conducted by standard carbodiimde chemistry. To a solution of PFV/PSMA NPs in B-R buffer (pH 5.0), EDC was directly added and the reaction mixture was stirred for 15 min. Then dopamine was added and the mixture was further stirred for 12 h in the dark at room temperature. Unreacted molecules were removed by centrifuge and washed with ultrapure water several times using microcentrifuge tube (MWCO = 100 kDa).

2.4. General procedure for pH determination in aqueous solution

A series of standard B-R pH buffered solutions were prepared by mixing 40 mM H_3PO_4, 40 mM acetic acid, 40 mM boric acid and 200 mM NaOH with various volume ratios. The specific pH values ranging from 5.0 to 9.0 were determined by Meitler Toledo FE20K pH-meter. The concentrated PFV/PSMA-DA NPs stock solution was then added into the above B-R buffer solution and incubated for 1 h. Finally, 200 μL of the resulting solution was transferred to a quartz cuvette and a fluorescence emission spectrum was obtained at room temperature.

To evaluate the reversibility of PFV/PSMA-DA nanoprobe, the pH of PFV/PSMA-DA solution between pH 5.0 and pH 9.0 was adjusted back and forth by adding 1 M HCl or NaOH.

2.5. Cytotoxicity assay

The cytotoxicity of PFV/PSMA-DA NPs toward the HeLa cells was measured by the methyl thiazolyl tetrazolium (MTT) assay. Human cervical cells (HeLa cells) were cultured in Dulbecco's modified Eagle's medium (DMEM). The medium were supplemented with 10% heat-inactivated fetal bovine serum (FBS) and relevant antibiotics (100 μg/mL streptomycin and 100 U/mL penicillin). HeLa cell lines were cultured at 37 °C in a 5% CO_2 incubator with humidified atmosphere. And then the cells were incubated with various concentrations of PFV/PSMA-DA NPs for 24 h. 50 μL MTT solution (5 mg/mL) was added to each well and the solution was incubated for another 4 h under the same conditions. After 200 μL of DMSO was added to each plate well, a multifunction microplate reader was used for measuring the absorbance of each well at 570 nm.

2.6. Determination of intracellular pH

HeLa cells were incubated with PFV/PSMA-DA NPs for 9 h at 37 °C. Afterwards, the cells were washed with PBS for three times to remove excessive PFV/PSMA-DA NPs. The cells were then treated with high K^+ buffer (30 mM NaCl, 120 mM KCl, 1 mM $CaCl_2$, 0.5 mM $MgSO_4$, 1 mM NaH_2PO_4, 5 mM glucose, and 20 mM HEPES) with various pH values in the presence of nigericin (10 μM) for 10 mins. The fluorescence images were recorded by Olympus Fluo-view 1000, and the pH calibration curve was constructed with OriginPro software.

One-photon and two-photon bioimaging were performed using confocal laser scanning microscopy with a fixed excitation wavelength of 405 nm and 800 nm respectively.

3. Results and discussion

3.1. Sensing mechanism

Our new SPNs-based pH assay by redox active dopamine is illustrated in Scheme 1. Poly(9,9′-dioctylfluorene-2,7-ylene-vinylene-*co*-*alt*-1,4-phenylene) (PFV) have been previously shown their excellent two photon absorption (TPA) cross sections, which makes them useful in acting as two-photon light harvesting probe for bioimaging (Shen et al., 2013). Here we further prepared PFV nanoparticles by reprecipitation method where the surface of the PFV nanoparticles was functionalized with carboxyl groups by blending PFV with a functional polymer (PSMA) during nanoparticle formation. Dopamine was covalently attached to -COOH groups on the surface of PFV/PSMA NPs with EDC used as cross-linking agent. It has been demonstrated that dopamine can show reversible fluorescence quenching ability toward fluorophores via energy and/or electron transfer process with the change of pH values (Ji et al., 2012; Medintz et al., 2010). Increasing the buffer pH from acidic to alkaline decreases the dopamine oxidation potential, which favors the oxidation of dopamine and consequently increases the concentration of quinones in the medium. Thus, as the pH was increased, increased concentration of quinone could enhance the fluorescence quenching of PFV/PSMA-DA NPs. On the contrary, the oxidation of dopamine could be dramatically reduced in acidic solution and strong fluorescence emission of PFV/PSMA-DA NPs solution could be observed. Thus, a sensitive fluorescent response of the PFV/PSMA-DA NPs to the pH changes can be expected.

3.2. Preparation and characterizations of PFV/PSMA-DA NPs

The PFV/PSMA-DA NPs were prepared using a method similar to the coprecipiation method as described previously (Yu et al., 2012). A

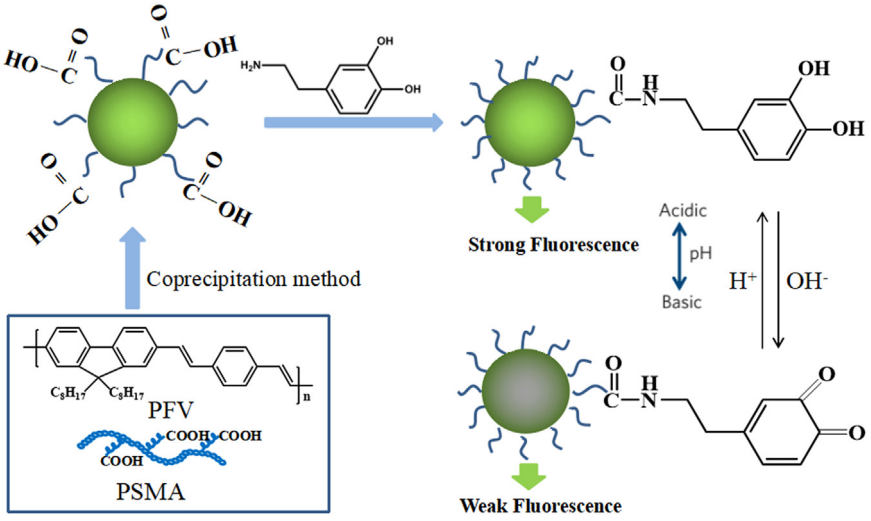

Scheme 1. Schematic representation of pH sensing based on PFV/PSMA-DA NPs.

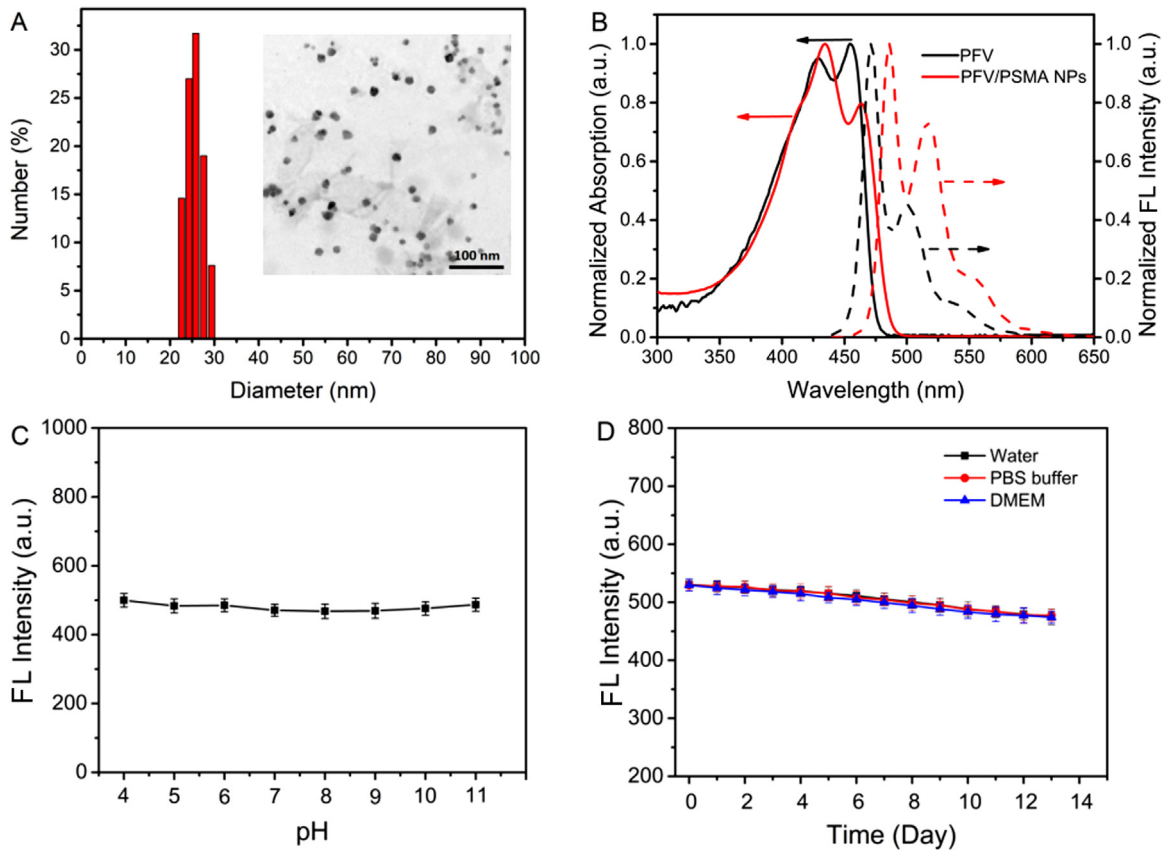

Fig. 1. (A) Hydrodynamic diameter and TEM image (inset) of PFV/PSMA-DA NPs. (B) Normalized UV–vis absorption and one photon fluorescence spectra of PFV in THF solution and PFV/PSMA-DA NPs in aqueous solution. The excitation wavelength is 435 nm. (C) Fluorescence intensity of PFV/PSMA NPs in B-R buffer solutions with different pH values. (D) Fluorescence intensity of PFV/PSMA-DA NPs ([PFV/PSMA-DA NPs] = 2.4 μg/mL) incubated in water, PBS buffer (pH 7.4), or DMEM for 13 days.

particle size analysis gained from dynamic light scattering (DLS) indicates that the majority of PFV/PSMA-DA NPs possess diameters in this range of 28 ± 3 nm (Fig. 1A). Transmission electron microscopy (TEM) result also demonstrates that PFV/PSMA-DA NPs generally form small nanoparticles with average diameter of about 15 nm (inset in Fig. 1A). The size difference could be attributed to the collapse and shrinkage of the nanoparticles in dry state. The particle size and morphologies of PFV/PSMA-DA NPs were further verified by SEM (Fig. S1A) and AFM (Fig. S1B), which indicate most of PFV/PSMA-DA NPs possess an average diameter of 17 nm and ~12 nm respectively. The size measurements are in accordance with each other and the particle height obtained from AFM should be slightly smaller than the lateral size obtained from TEM results. Fig. 1B shows the UV–vis absorption and one-photon fluorescence spectra of nanoparticles. The absorption spectra are slightly broadened compared to the polymer in THF solution, which is consistent with previous reports (Bao et al., 2014). The

nanoparticles also exhibit a red-shifted fluorescence as compared to the polymer in organic solvent, which is due to the increased interchain interactions and multiple energy transfer in nanoparticles (Wu et al., 2008). Furthermore, the intensity of fluorescence emission from PFV/PSMA NPs without dopamine functionalization in B-R buffer with various pH values was also investigated. As shown in Fig. 1C, the fluorescence intensity of PFV/PSMA NPs shows no obvious changes with different pH values, which clearly demonstrates that dopamine plays a crucial role in the pH-dependent fluorescence quenching of PFV/PSMA-DA NPs and ensure the pH sensing ability of PFV/PSMA-DA NPs. To evaluate the fluorescence stability of PFV/PSMA-DA NPs, the fluorescence intensity of PFV/PSMA-DA NPs in water, phosphate-buffered saline (PBS, pH 7.4), or Dulbecco's Modified Eagle Medium (DMEM) for 13 days was investigated. As shown in Fig. 1D, the fluorescence intensity of the nanoparticles shows no obvious changes both in PBS and DMEM during 13-day study duration, which is more stable than small molecule fluorescent dyes and indicates that PFV/PSMA-DA NPs is beneficial for bioimaging and biosensing.

3.3. pH sensing performance of PFV/PSMA-DA NPs

We now focus on the pH sensing performance of PFV/PSMA-DA NPs in B-R buffer with different pH values. As shown in Fig. 2A, the fluorescence intensity of PFV/PSMA-DA NPs exhibits gradually enhancement with the decrease of pH values. The calibration curve of pH values are given in Fig. 2B, showing a good linear relationship (R^2 = 0.9935) in the pH range from 5.0 to 9.0. The reversibility of PFV/PSMA-DA nanoprobe was then assessed. As shown in Fig. 2C, the fluorescence intensity of PFV/PSMA-DA NPs can exhibit a progressive recovery that is also pH-dependent, and this reversible cycle can be retained for at least 5 times between pH 5.0 and pH 9.0. The cytotoxicity of PFV/PSMA-DA NPs was subsequently evaluated using standard MTT assay. As shown in Fig. 2D, PFV/PSMA-DA NPs has no obvious effect on the cell viability after incubation for 24 h, indicating that PFV/PSMA-DA NPs are noncytotoxic due to the favorable biocompatibility of semiconducting polymer and dopamine.

3.4. Imaging of intracellular pH variation

Furthermore, considering the sensitive fluorescence response to pH values and low cytotoxicity, nanoprobe PFV/PSMA-DA NPs were used for intracellular pH measurement. The intracellular calibration experiments were performed in high-K^+ HEPES-buffered solution containing 10 μM nigericin. Nigericin is an H^+/K^+ ionophore, which could help equilibrate the intracellular and extracellular pH. As described in Fig. 3A, the green fluorescence intensity of PFV/PSMA-DA NPs gradually increases with the decrease of pH value from 9.0 to 5.0. Fig. 3B shows that the average fluorescence intensity of PFV/PSMA-DA NPs response sensitively to intracellular pH, which generates a good linear relationship in the pH range from 5.0 to 9.0. Furthermore, flow cytometry measurements were performed to verify the successful sensing of intracellular pH changes by PFV/PSMA-DA NPs. Consistent with the confocal laser scanning microscopy (CLSM) results, cells exhibit significant emission enhancement upon decreasing the pH of the incubation medium from 9.0 to 5.0 (Fig. 3C). The similar pH response of PFV/PSMA-DA NPs in flow cytometry and confocal imaging confirms the

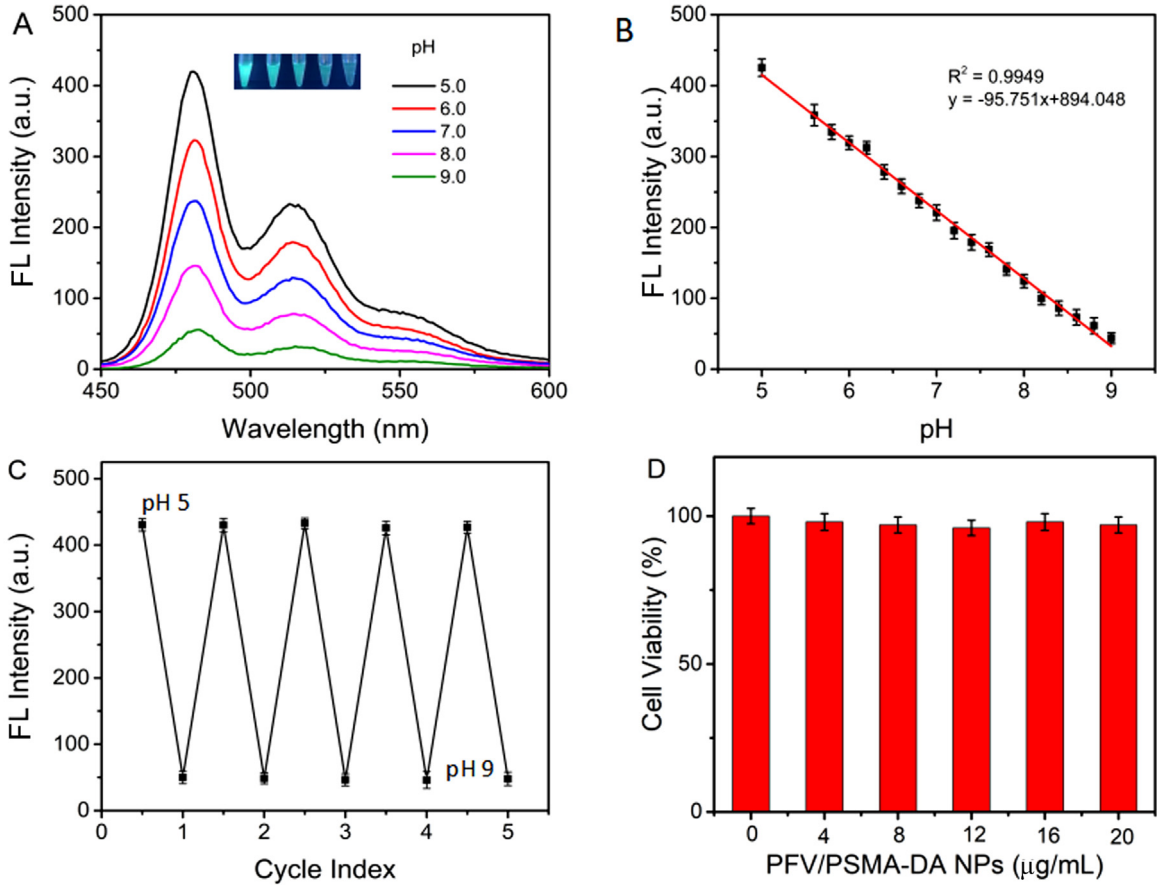

Fig. 2. (A) Fluorescence spectra of PFV/PSMA-DA NPs in B-R buffers at various pH values. [PFV/PSMA-DA NPs] = 2 μg/mL. (B) Linear relationship between fluorescence intensity and pH values in the range of 5.0–9.0. (C) pH reversibility assess of PFV/PSMA-DA NPs between pH 5.0 and 9.0. The cycles were repeated for five times. (D) Cell viability of HeLa cells treated with PFV/PSMA-DA NPs for 24 h. The viability of the control cells (0 μg/mL PFV/PSMA-DA NPs) was considered 100%. All error bars represent the standard deviation determined from six independent assays.

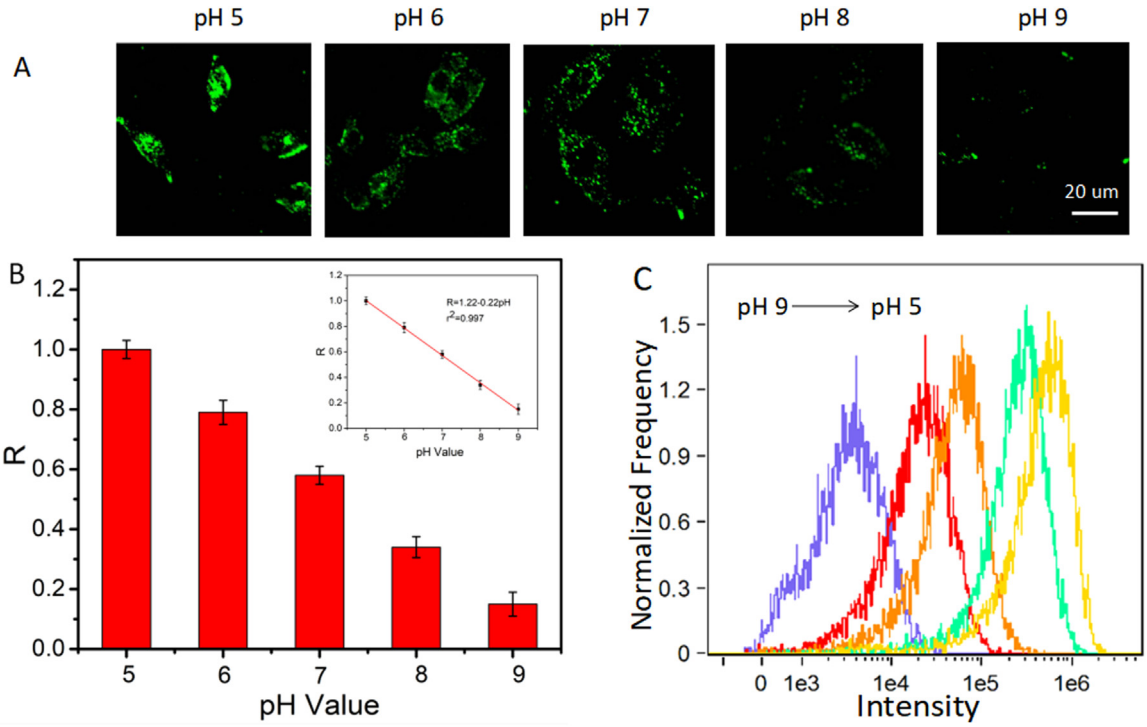

Fig. 3. (A) One-photon CLSM image of PFV/PSMA-DA NPs in HeLa cells at pH values of 5.0, 6.0, 7.0, 8.0 and 9.0, respectively. (B) Corresponding histograms of the fluorescence intensity ratio (R) of the pH range from 9.0 to 5.0 (R = fluorescence intensity at pH 5.0–9.0/fluorescence intensity at pH 5.0). Inset presents the linear relationship between R and pH values in the pH range from 5.0–9.0. The error bars indicate the standard deviation determined from three independent measurements. (C) Flow cytometry measurements of the intensity distributions of PFV/PSMA-DA NPs in HeLa cells at pH values of 5.0, 6.0, 7.0, 8.0 and 9.0, respectively.

effectiveness of this nanoprobe to accurately detect intracellular pH changes.

3.5. Quantitative measurement of intracellular pH fluctuations

To further demonstrate the sensing capability of PFV/PSMA-DA NPs to different stimulus, HeLa cells were treated by redox substances such as NAC (N-acetylcysteine, a GSH precursor) and H_2O_2 according to previously reports (Ma et al., 2016; Shi et al., 2012). First, HeLa cells were incubated only with PFV/PSMA-DA NPs, serving as the control group. As shown in Fig. 4, the averaged intracellular pH value of intact HeLa cells is measured to be 6.85 ± 0.15 according to the calibration curve. The intracellular pH value was measured to be 7.20 ± 0.25 after the cells incubating with H_2O_2, which indicates that H_2O_2 makes the HeLa cells more basic due to generation of oxidative stress and increase of pH value in lysosomes (Ma et al., 2016). On the contrary, NAC can acidify HeLa cells to pH 5.12 ± 0.25. This phenomenon is consistent with previous report, which has been ascribed to reductive cellular environment caused by the activation of lysosomal V-ATPase. (Ma et al., 2016) In general, the excellent reproducibility of our strategy allows the quantitative detection of intracellular pH changes under different stimulus.

3.6. Two-photon imaging of intracellular pH variation

Such nanosized pH sensor based on semiconducting polymers have a great potential in application of sensing pH and detecting cancer cells in biological tissue. We therefore performed the two-photon imaging to further investigate the intracellular pH sensing of PFV/PSMA-DA NPs under the same experimental conditions as in one-photon fluorescence microscopy. As shown in Fig. 5A and B, the fluorescence intensity of PFV/PSMA-DA NPs is gradually enhanced with the decrease of pH, exhibiting a linear response to pH from 9.0 to 5.0. Fig. 5C shows the two-photon fluorescence imaging of HeLa cells treated with H_2O_2 and

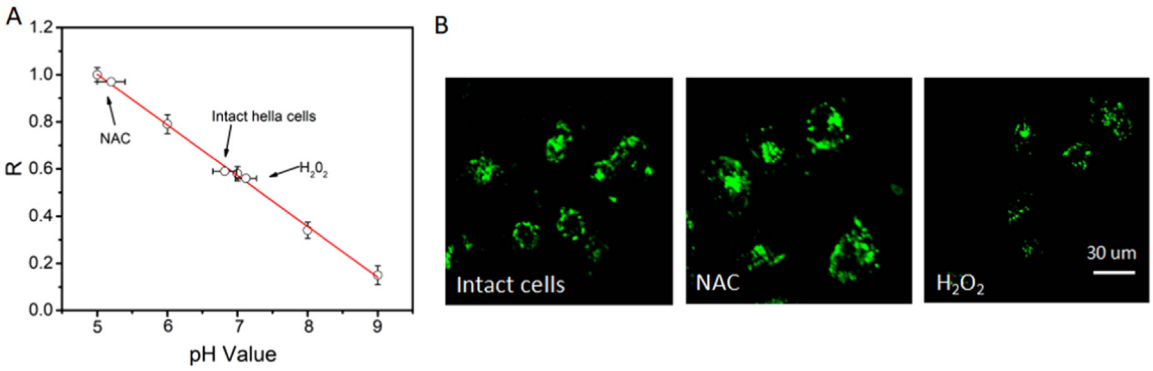

Fig. 4. (A) Intracellular pH calibration curve of PFV/PSMA-DA NPs in HeLa cells. (B) CLSM images of HeLa cells loaded with PFV/PSMA-DA NPs. Intact cells, cells treated with NAC (100 mM) and H_2O_2 (100 mM) for 1 h at 37 °C.

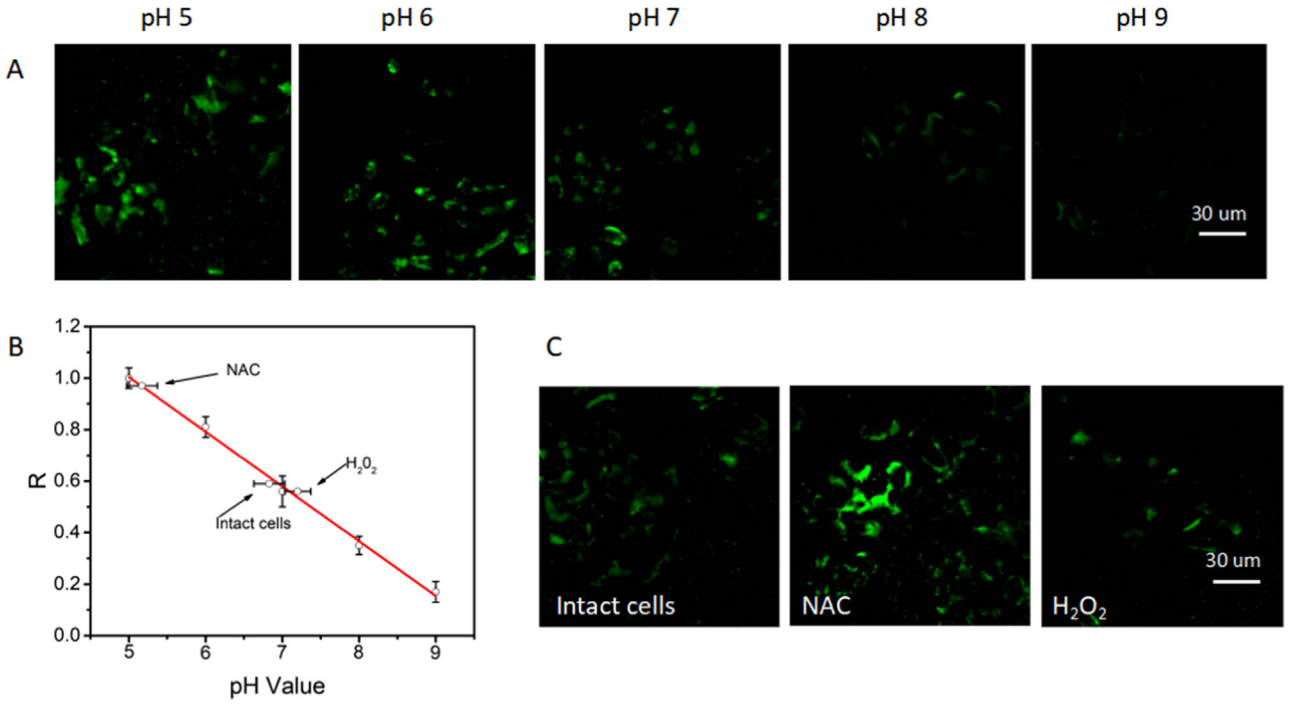

Fig. 5. (A) Two-photon fluorescence images of PFV/PSMA-DA NPs in HeLa cells at pH values of 5.0, 6.0, 7.0, 8.0 and 9.0, respectively. (B) Intracellular pH calibration curve of two-photon fluorescence intensity of PFV/PSMA-DA NPs in HeLa cells (R = fluorescence intensity at pH 5.0–9.0/fluorescence intensity at pH 5.0). (C) Two-photon fluorescence images of HeLa cells loaded with PFV/PSMA-DA NPs. Intact cells, cells treated with NAC (100 mM) and H_2O_2 (100 mM) for 1 h at 37 °C.

NAC, respectively. Compared with the fluorescence intensity of control cells, the fluorescence intensity of H_2O_2 treated cells is decreased. And the addition of NAC causes a decrease in cellular pH, which is reflected by the enhanced two photon fluorescence intensity. These data are in good agreement with results obtained from one-photon fluorescence CLSM imaging, which indicates that PFV/PSMA-DA NPs is suitable for imaging pHi in living cells as a two-photon excited fluorescent nanosensor.

4. Conclusion

In summary, a semiconducting polymer-based, two-photon excited fluorescence turn-on sensor PFV/PSMA-DA NPs with excellent biocompatibility and stability was developed for intracellular pH imaging in living cells. Both one- and two-photon fluorescence intensity of the nanoprobe are enhanced gradually with the decrease of intracellular pH values and also shows good linear relationships with pHi changes. Compared to untreated cells, the nanoprobe can sensitively reflect the stimulus-induced pH changes by H_2O_2 and NAC, respectively. The consistent results obtained from one- and two-photon cell imaging experiments demonstrate that PFV/PSMA-DA NPs is a promising two-photon fluorescent probe for pH sensing.

Acknowledgements

This work was financially supported by the National Natural Science Foundation of China (21574069, 21475064), the National Key Research and Development Program of China (2017YFA0205302), the Program for Changjiang Scholars and Innovative Research Team in University (IRT_15R37), and the Natural Science Foundation of Jiangsu Province (BK20151503).

Appendix A. Supporting information

Supplementary data associated with this article can be found in the online version at doi:10.1016/j.bios.2018.10.027.

References

Bao, B.Q., Ma, M.F., Chen, J., Yuwen, L.H., Weng, L.X., Fan, Q.L., Huang, W., Wang, L.H., 2014. ACS Appl. Mater. Inter. 6 (14), 11129–11135.
Bao, B.Q., Ma, M.F., Zai, H.F., Zhang, L., Fu, N.N., Huang, W., Wang, L.H., 2015. Adv. Sci. 2 (3), 140009.
Bruni, F., Pedrini, J., Bossio, C., Santiago-Gonzalez, B., Meinardi, F., Bae, W.K., Klimov, V.I., Lanzani, G., Brovelli, S., 2017. Adv. Funct. Mater. 27 (12), 160553.
Chen, L., Wu, L., Yu, J., Kuo, C.T., Jian, T., Wu, I.C., Rong, Y., Chiu, D.T., 2017. Chem. Sci. 8 (10), 7236–7245.
Dennis, A.M., Rhee, W.J., Sotto, D., Dublin, S.N., Bao, G., 2012. ACS Nano 6 (4), 2917–2924.
Derfus, A.M., Chan, W.C.W., Bhatia, S.N., 2004. Nano Lett. 4 (1), 11–18.
Hou, J.T., Ren, W.X., Li, K., Seo, J., Sharma, A., Yu, X.Q., Kim, J.S., 2017. Chem. Soc. Rev. 46 (8), 2076–2090.
Ji, X., Palui, G., Avellini, T., Na, H.B., Yi, C.Y., Knappenberger, K.L., Mattoussi, H., 2012. J. Am. Chem. Soc. 134 (13), 6006–6017.
Jiang, M.J., Gu, X.G., Lam, J.W.Y., Zhang, Y.L., Kwok, R.T.K., Wong, K.S., Tang, B.Z., 2017. Chem. Sci. 8 (8), 5440–5446.
Jung, S., Chen, X.Y., 2018. Adv. Healthc. Mater. 7 (14), 1800252.
Ke, C.S., Fang, C.C., Yan, J.Y., Tseng, P.J., Pyle, J.Y., Chen, C.P., Zhang, X., Chan, Y.H., 2017. ACS Nano 11 (3), 3166–3177.
Kim, H.M., Cho, B.R., 2015. Chem. Rev. 115 (11), 5014–5055.
Li, D., Xu, H., Li, D., Wang, Y.H., 2017. Talanta 166, 54–62.
Li, J., Lim, C.S., Kim, G., Kim, H.M., Yoon, J., 2017. Anal. Chem. 89 (16), 8496–8500.
Ma, Y., Liang, H., Zeng, Y., Yang, H., Ho, C.L., Xu, W., Zhao, Q., Huang, W., Wong, W.Y., 2016. Chem. Sci. 7 (5), 3338–3346.
Medintz, I.L., Stewart, M.H., Trammell, S.A., Susumu, K., Delehanty, J.B., Mei, B.C., Melinger, J.S., Blanco-Canosa, J.B., Dawson, P.E., Mattoussi, H., 2010. Nat. Mater. 9 (8), 676–684.
Miesenbock, G., De Angelis, D.A., Rothman, J.E., 1998. Nature 394 (6689), 192–195.
Nareoja, T., Deguchi, T., Christ, S., Peltomaa, R., Prabhakar, N., Fazeli, E., Perala, N., Rosenholm, J.M., Arppe, R., Soukka, T., Schaferling, M., 2017. Anal. Chem. 89 (3), 1501–1508.
Peng, H.S., Chiu, D.T., 2015. Chem. Soc. Rev. 44 (14), 4699–4722.
Qian, L.H., Li, L., Yao, S.Q., 2016. Acc. Chem. Res. 49 (4), 626–634.
Shen, X., Li, L., Chan, A.C.M., Gao, N., Yao, S.Q., Xu, Q.H., 2013. Adv. Opt. Mater. 1 (1), 92–99.
Shi, W., Li, X.H., Ma, H.M., 2012. Angew. Chem. Int. Ed. 51 (26), 6432–6435.
Sun, J., Mel, H., Wang, S., Gao, F., 2016. Anal. Chem. 88 (14), 7372–7377.
Sun, J.Y., Mei, H., Gao, F., 2017a. Biosens. Bioelectron. 91, 70–75.
Sun, J.Y., Ling, P.H., Gao, F., 2017b. Anal. Chem. 89 (21), 11703–11710.
Sun, W., Guo, S.G., Hu, C., Fan, J.L., Peng, X.J., 2016. Chem. Rev. 116 (14), 7768–7817.

Tantama, M., Hung, Y.P., Yellen, G., 2011. J. Am. Chem. Soc. 133 (26), 10034–10037.
Thomas, J.A., 2015. Chem. Soc. Rev. 44 (14), 4494–4500.
Wang, P., Zhang, C., Liu, H.W., Xiong, M.Y., Yin, S.Y., Yang, Y., Hu, X.X., Yin, X., Zhang, X.B., Tan, W.H., 2017. Chem. Sci. 8 (12), 8214–8220.
Wen, Q.S., Liu, L.B., Yang, Q., Lv, F.T., Wang, S., 2013. Adv. Func. Mater. 23 (6), 764–769.
Wu, C., Bull, B., Szymanski, C., Christensen, K., McNeill, J., 2008. ACS Nano 2 (11), 2415–2423.
Wu, C., Chiu, D.T., 2013. Angew. Chem. Int. Ed. 52 (11), 3086–3109.
Xu, W., Zeng, Z.B., Jiang, J.H., Chang, Y.T., Yuan, L., 2016. Angew. Chem. Int. Ed. 55 (44), 13658–13699.
Yin, J., Hu, Y., Yoon, J., 2015. Chem. Soc. Rev. 44 (14), 4619–4644.
Yu, J., Wu, C., Zhang, X., Ye, F., Gallina, M.E., Rong, Y., Wu, I.C., Sun, W., Chan, Y.H., Chiu, D.T., 2012. Adv. Mater. 24 (26), 3498–3504.
Yu, J.B., Rong, Y., Kuo, C.T., Zhou, X.H., Chiu, D.T., 2017. Anal. Chem. 89 (1), 42–56.